Lattice anharmonicity, phonon dispersion, and thermal conductivity of PbTe studied by the phonon quasiparticle approach

Yong Lu,[1,2] Tao Sun,[3] and Dong-Bo Zhang[2,4,*]

[1]*Beijing University of Chemical Technology, College of Science, Beijing 100029, China*
[2]*Beijing Computational Science Research Center, Beijing 100194, China*
[3]*Key Laboratory of Computational Geodynamics, University of Chinese Academy of Sciences, Beijing 100049, China*
[4]*College of Nuclear Science and Technology, Beijing Normal University, Beijing 100875, China*

(Received 23 December 2017; revised manuscript received 1 April 2018; published 25 May 2018)

We investigated the vibrational property of lead telluride (PbTe) with a focus on lattice anharmonicity at moderate temperatures ($300 < T < 800$ K) using the phonon quasiparticle approach which combines first-principles molecular dynamics and lattice dynamics. The calculated anharmonic phonon dispersions are strongly temperature dependent and some phonon modes adopt giant frequency shifts, e.g., transverse optical modes in the long-wavlength regime. As a result, we witness the avoided crossing between transverse optical modes and longitudinal acoustic modes at elevated temperature, in good agreement with experimentation and available theoretical studies. These results, together with the large root-mean-square displacements of atoms, reveal a strong anharmonic effect in PbTe. The obtained phonon lifetimes allow studies of transport properties. For considered temperatures, the phonon mean free paths can be shorter than lattice constants at relatively high temperature, especially for optical modes. This finding goes against the widely employed minimal phonon mean free path concept. As such, the calculated lattice thermal conductivity of PbTe, which is indeed relatively small, does not have the prescribed minima at high temperature, showcasing the breakdown of the minimal mean free path theory. Our study provides a basis for delineating vibrational and transport properties of PbTe and other thermoelectric materials within the framework of the phonon gas model.

DOI: 10.1103/PhysRevB.97.174304

I. INTRODUCTION

Thermoelectricity provides a channel for conversion between thermal and electric energies. Seeking materials with excellent thermoelectric performance is a fundamental task of today's materials science studies. In general, the efficiency of a thermoelectric system is characterized using the so-called figure of merit [1,2],

$$ZT = \sigma S^2 T/(\kappa_{\rm ele} + \kappa_{\rm lat}), \tag{1}$$

where S, T, and σ are Seebeck coefficient, temperature, and electric conductivity, respectively. $\kappa_{\rm ele}$ and $\kappa_{\rm lat}$ are electronic thermal conductivity and lattice thermal conductivity, respectively. Therefore, for an ideal thermoelectric system, not only a large value of S and high electric conductivity are needed, but low thermal conductivity ($\kappa_{\rm ele} + \kappa_{\rm lat}$) is also a necessity. Because $\kappa_{\rm ele}$ is usually negligibly small in semiconductor systems, $\kappa_{\rm lat}$ is the key quantity to reduce in order to obtain good ZT [3–5]. Therefore, understanding the formation of $\kappa_{\rm lat}$ against the underlying microscopic mechanism is of fundamental importance in elucidating the thermoelectric property of a system. Usually, $\kappa_{\rm lat}$ of a crystalline material is evaluated by Peierls-Boltzmann theory [6–9],

$$\kappa_{\rm lat} = \frac{1}{3N}\sum_{\mathbf{q},s} c_{\mathbf{q},s} v_{\mathbf{q},s} l_{\mathbf{q},s}, \tag{2}$$

where N is the number of unit cells in the crystal, $c_{\mathbf{q},s}$, $v_{\mathbf{q},s}$, and $l_{\mathbf{q},s}$ are heat capacity, group velocity, and phonon mean free path, respectively, for mode $(\mathbf{q},s)$ indexed with wave vector $\mathbf{q}$ and branch s, and

$$l_{\mathbf{q},s} = \tau_{\mathbf{q},s} v_{\mathbf{q},s}, \tag{3}$$

where $\tau_{\mathbf{q},s}$ is the phonon lifetime.

PbTe is a representative thermoelectric material suitable for operations at moderate temperature and is believed to be an excellent alternative for materials obtained via structure engineering [10–14]. As a distinct feature, PbTe has a very low bulk thermal conductivity, e.g., $\kappa_{\rm lat} \simeq 2$ W m^{-1} K^{-1} at 300 K [15,16]. The understanding mainly relies on an anharmonic mechanism. This was first proposed by a seminal experimental study [17], where a strong phonon-phonon interaction between the longitudinal acoustic (LA) branch and the transverse optical (TO) branch was revealed by inelastic neutron scattering measurements. This finding has stimulated intense theoretical investigations of the lattice anharmonicity of PbTe at finite temperatures [18–20]. Within the domain of the phonon picture, first-principles-based approaches provide an excellent paradigm for delineating anharmonic effects on phonon spectra. For example, by fitting the first-principles potential surface obtained at finite temperature to an effective harmonic potential, several groups successfully reproduced the anomalous phonon spectra obtained in experiments [19,20]. Nonetheless, the understanding of $\kappa_{\rm lat}$ from first-principles calculations is not sufficient yet. Although the many-body perturbation approach is effective for weakly anharmonic systems, the treatment of strongly anharmonic systems such

*Corresponding author: dbzhang@csrc.ac.cn

as PbTe, where higher orders of anharmonic effect may play an important role, is nontrivial. Indeed, a perturbation approach based on a three-phonon process may overestimate $\kappa_{\rm lat}$ at high temperature [21]. Due to strongly anharmonic effects, not only the phonon lifetimes are short, but the group velocities of phonons as in Eq. (2) also display heavy temperature dependence.

Indeed, it is a theoretical task to seek consistent solutions between anharmonic phonon spectra and thermal conductivity. This can be accomplished by employing the concept of phonon quasiparticles which quantitatively characterize the anharmonic effect with a renormalized frequency ($\widetilde{\omega}_{\mathbf{q},s}$) and linewidth ($\Gamma_{\mathbf{q},s}$). Then the phonon lifetime can be obtained from the phonon linewidth using the relationship of $\tau_{\mathbf{q},s} \simeq 1/2\Gamma_{\mathbf{q},s}$ within the relaxation-time approximation.

Therefore, both phonon spectra and thermal conductivity can be derived once phonon quasiparticles are known. Here, we employ a recent theoretical advance which offers the capability to numerically depict phonon quasiparticles from first-principles calculations [22,23], and with this approach, we investigate the vibrational property of PbTe. Our calculations first demonstrate the dynamical stability of cubic PbTe from the probability distribution of atomic displacement in real space, and also from the numerical description of phonon quasiparticles in phase space. These analyses also confirm the validity of the phonon picture in PbTe. We next show the giant frequency shifts of the transverse optical branch with temperature, especially for those modes around the Brillouin zone center. This result, once again, confirms previous experimental findings [19,24]. Consequently, we find that the group velocities of those modes belonging to the transverse optical branch are also temperature sensitive. These results reveal the strong anharmonic effect in PbTe. The calculated phonon lifetimes allow one to study transport properties. Note that although the relaxation-time approximation based on third-order perturbation theory does not include the effect of frequency shifts, it is included naturally in our approach. Surprisingly, the obtained phonon mean free paths can be shorter than the lattice constants for some modes even at relatively low temperatures, indicating the breakdown of the minimal mean free path theory. The obtained lattice thermal conductivity compares well with experiments [25,26].

II. METHODS AND COMPUTATIONAL DETAILS

A phonon quasiparticle can be numerically depicted with the velocity autocorrelation function (VAF) of mode-projected velocity [22],

$$\langle \mathbf{V}(0)\cdot\mathbf{V}(t)\rangle_{\mathbf{q},s} = \lim_{t_0\to\infty}\frac{1}{t_0}\int_0^{t_0}\mathbf{V}_{\mathbf{q},s}(t')\mathbf{V}_{\mathbf{q},s}(t'+t)dt', \quad (4)$$

and the mode-projected velocity of normal mode ($\mathbf{q}$,s) is

$$\mathbf{V}_{\mathbf{q},s}(t) = \sum_{j=1}^{N}\mathbf{V}_j(t)e^{-i\mathbf{q}\cdot\mathbf{R}_j}\cdot\hat{e}_{\mathbf{q},s}, \quad (5)$$

where $\mathbf{V}_j(t) = \mathbf{v}_j(t)\sqrt{M_j}$ is the mass weighted velocity and $\mathbf{v}_j(t)$ $(j = 1,\ldots,N)$ are atomic velocities obtained from first-principles molecular dynamics (MD) with N atoms per supercell. $\hat{e}_{\mathbf{q},s}$ is the polarization vector of the harmonic phonon of mode ($\mathbf{q}$,s), which can be routinely obtained by performing phonon calculations with standard approaches such as density functional perturbation theory [27,28]. M_j and $\mathbf{R}_j$ are the atomic mass and coordinates of atom j in the supercell. For a well-defined phonon quasiparticle, VAF decays in an oscillatory way, and the power spectrum $G_{\mathbf{q},s}(\omega)$, i.e., the Fourier transform of VAF,

$$G_{\mathbf{q},s}(\omega) = \int_0^{\infty}\langle \mathbf{V}(0)\cdot\mathbf{V}(t)\rangle_{\mathbf{q},s}e^{i\omega t}dt, \quad (6)$$

follows a Lorantzian-type line shape. Both the renormalized phonon frequency $\widetilde{\omega}_{\mathbf{q},s}$ and linewidth $\Gamma_{\mathbf{q},s}$ can be extracted from $G_{\mathbf{q},s}$.

TABLE I. The MD simulation volumes [V (Å^3/f.u.)] at different temperatures [T (K)]. The equilibrium volume at 0 K is obtained by volume relaxation using VASP. The temperature-dependent volumes are obtained by incorporating the experimental lattice thermal expansion in Ref. [39].

T	0	300	400	500	600	700	800
$V(T)$	70.57	71.78	72.27	72.69	73.16	73.59	74.02

The first-principles MD simulations on the 4×4×4 supercell (128 atoms) of cubic PbTe are carried out using density functional theory with the projected-augmented-wave (PAW) method [29] as implemented in the VASP package [30]. The electron exchange and correlation potential is described by the generalized gradient approximation with Perdew, Burke, and Ernzerhof (PBE) form [31]. The plane-wave cutoff is set to 350 eV and Fermi-Dirac smearing corresponding to the simulation temperature is adopted. A 2×2×2 k-point grid with the Monkhorst-Pack scheme is used for the Brillouin zone sampling [32]. Simulations are carried out considering temperatures from 300 to 800 K and a series of different volumes $70.57 < V < 75.19$ Å^3 where the lattice constant is $6.56 < l_0 < 6.70$ Å. This volume range covers static pressures $-2.2 < P < 0$ GPa. For the MD simulations at constant volume (V_0), the relaxed volume of 70.57 Å^3 by VASP is fixed. While for constant pressure ($P = 0$ GPa) conditions, we obtain the dependence of volume and temperature according to the experimental lattice thermal expansion in Ref. [33]. The simulation volumes at different temperatures are listed in Table I. We use a 1 fs time step and set the temperature with the Nosé thermostat [34]. To minimize statistical error, five parallel MD simulations are performed at each temperature. Each MD runs for about 50 ps. Harmonic phonon dispersions and polarization vectors are calculated using the density functional perturbation theory (DFPT) [27,28] as implemented in the QUANTUM-ESPRESSO (QE) package [35]. A plane-wave basis is terminated by an 80 Ry energy cutoff, and a 16×16×16 k mesh is used for the Brillouin zone (BZ) integration for electronic self-consistent calculations of PbTe primitive cells. We performed convergence tests with larger cutoff or k mesh but found negligible differences in phonon frequencies. The pseudopotential forms with the PAW method and PBE exchange and correlation functional are used in the QE calculations, the same as that in VASP. The phonon dispersion relations are obtained using a uniform 4×4×4 $\mathbf{q}$ mesh.

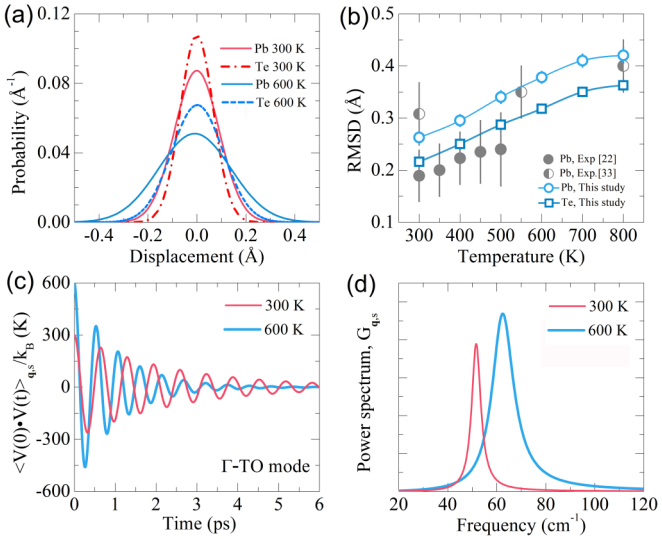

FIG. 1. (a) Probability distributions of atomic displacements along the x direction with respect to the ideal cubic structure at different temperatures for both Pb and Te atoms. (b) Root-mean-squared displacements (RMSD) of Pb and Te atoms. The experimental results of Božin *et al.* [24] and Kastbjerg *et al.* [33] are shown for comparison. (c) $\langle \mathbf{V}(0) \cdot \mathbf{V}(t) \rangle_{\mathbf{q},s}$ and (d) power spectrum $G_{\mathbf{q},s}$ for the TO mode at the Γ point obtained at 300 and 600 K, respectively.

III. RESULTS AND DISCUSSIONS

A. Dynamic stability and phonon quasiparticles

Thermally induced lattice distortion in PbTe has been observed in experiments [24,33]. The x-ray total scattering studies suggest an off-centering atomic displacement of ∼ 0.19 Å along ⟨100⟩ at 300 K [24]. In a recent experimental study based on synchrotron powder x-ray diffraction data analyzed with the maximum entropy method, even larger displacements of ∼0.3 Å are predicted for Pb at 300 K [33]. The large amplitude of atomic displacements might give rise to heavy lattice anharmonicity.

We have calculated the probability distributions of atomic displacements and the root-mean-square displacements from first-principles MD simulations under constant volume conditions ($V_0 = 70.57$ Å^3) with zero static pressure. Figure 1(a) shows the probability distributions of atomic displacements along the x direction with respect to the perfect cubic structure under constant volume conditions. Note that due to the cubic symmetry, the probability distributions of atomic displacements are identical in the three Cartesian directions. For all the temperatures, bell-shaped distribution curves are centered at the zero displacement for both Pb and Te, and the distribution functions broaden with temperature. Because the probability distribution of atomic displacements is maximal at the equilibrium position around which the atom oscillates, we conclude that the cubic lattice is the equilibrium structure for PbTe, consisting well with previous observations by the pair distribution function analysis [36]. These findings are in agreement with recent experimental studies performed by an extended x-ray absorption fine structure spectroscopy [37] and the high-resolution neutron powder diffraction [38].

To quantitatively depict the oscillation amplitude, we calculate the root-mean-square displacements of Pb and Te atoms. The results are shown in Fig. 1(b). The root-mean-square displacements are overall large and increase with temperature. Nonlinear dependence on temperature can be identified at $T > 400$ K, a feature beyond the scope of the third-order many-body perturbation theory [39]. At 300 K, the root-mean-square displacement of Pb is ∼0.26 Å, consistent with the experimental observation of 0.19 ± 0.05 Å [24] and 0.31 ± 0.06 Å [33]. The root-mean-square displacements of Pb are always larger than those of the Te atom at all the temperatures.

Note that the previous first-principles calculations suggest that the abnormally large-amplitude thermal vibrations stem from a delicate competition of dual ionicity and covalency [36]. Here, we further demonstrate the dynamical stability of cubic PbTe in the phase space, where the VAF, i.e., phonon quasiparticles, associates the atomic displacements with phonon power spectrum. For example, Fig. 1(c) shows the VAFs of one transverse optical (TO) mode at the Γ point [$\mathbf{q} = (0,0,0)$] with a harmonic frequency of 28.12 cm^{-1} at different temperatures. Both display oscillatory decaying behaviors, a sign of structural stability. Note that the VAF decays faster at 600 K than at 300 K. Correspondingly, the associated power spectra shown in Fig. 1(d) are of well-defined Lorentzian line shape with single peak, allowing us to identify the phonon frequencies and linewidths of this mode at different temperatures: $\widetilde{\omega}_{\mathbf{q},s} = 51.54$ cm^{-1} and $\Gamma_{\mathbf{q},s} = 4.51$ cm^{-1} at 300 K and $\widetilde{\omega}_{\mathbf{q},s} = 62.20$ cm^{-1} and $\Gamma_{\mathbf{q},s} = 10.70$ cm^{-1} at 600 K. The enhanced phonon linewidths with temperature is consistent with the broadening atomic distribution functions with temperature in the real space.

B. Anharmonic phonon dispersion and frequency shifts

With the renormalized phonon frequencies $\widetilde{\omega}_{\mathbf{q},s}$ extracted from the small number of $\mathbf{q}$ sampled in MD simulations, our approach allows one to calculate the anharmonic phonon dispersion over the whole Brillouin zone [22,40]. The results are summarized in Fig. 2. Figure 2(a) shows the obtained anharmonic phonon dispersion at 300 K. The experimental data of the phonon frequencies of the whole LA branch and the phonon frequency of the TO mode at the Γ point obtained with inelastic neutron scattering at the same temperature [17] are also shown. It can be seen that our results agree well with experiments and capture the observed TO hardening at finite temperature. On the contrary, harmonic approximation based DFTP calculations both at the volume at 0 K and the volume at 300 K fail to capture the hardening of the TO mode. The volume at 300 K is 71.78 Å^3, the same as that in MD simulations at 300 K. At this volume, the temperature effect on phonon frequencies is accounted for through the temperature induced volumetric expansion [39,41]. Although the PBE overestimates the volumes of PbTe with respect to experiments, it can still successfully produce the softening of the TO mode and also other lattice and thermal properties, such as the heat capacity and entropy [41], elastic constants [42], and thermal resistivity [20]. In addition, the lattice thermal expansion considered in the present study is lower than that predicted by quasiharmonic approximation (QHA) [39,41]. For example, the lattice parameter of 6.597 Å at 300 K in

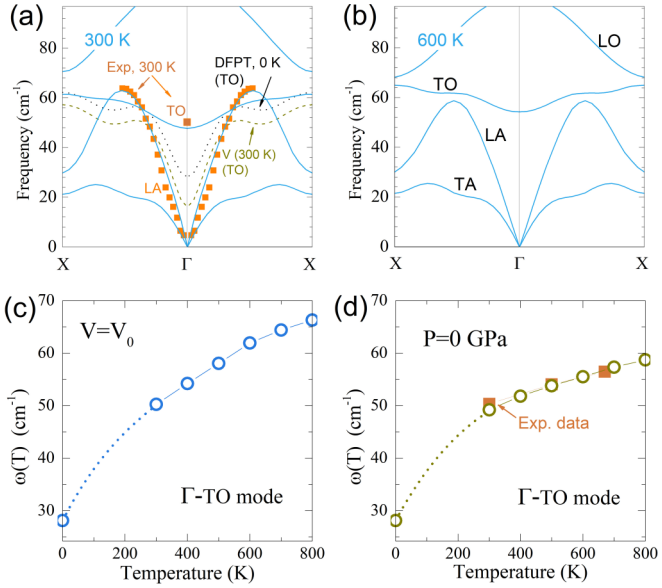

FIG. 2. Anharmonic phonon dispersions PbTe (a) at 300 K and (b) 600 K under constant pressure conditions where $P = 0$ GPa. In (a), the experimental phonon frequencies of the TO mode at the Γ point and the LA modes along the whole branch obtained from inelastic neutron scattering at 300 K [17] are shown in square dots. The phonon dispersion for the TO branch calculated by DFPT at the volume V at 0 K (dotted curve) and at volume V at 300 K (dashed curve) are also shown for comparison. (c) Frequency shift of the TO mode at the Γ point under constant volume conditions where the static pressure is zero. (d) Frequency shift of the same mode under constant pressure conditions with $P = 0$ GPa. The experimental result is shown for comparison.

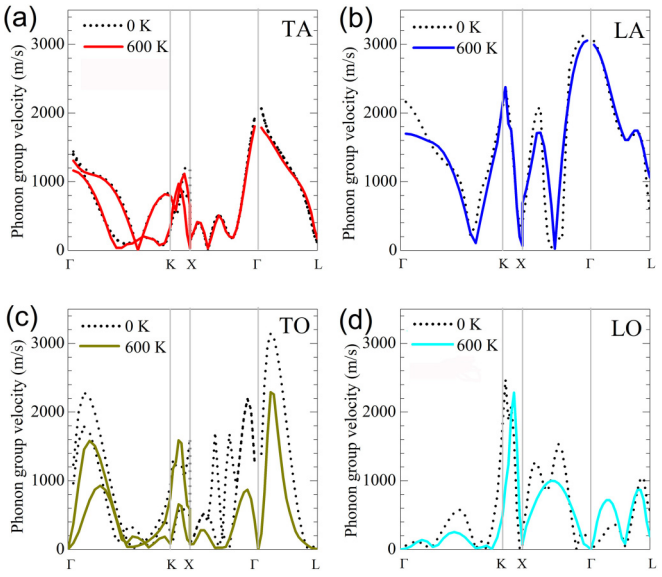

FIG. 3. Phonon group velocity (m/s) of (a) TA, (b) LA, (c), TO, and (d) LO modes for PbTe along high-symmetry points in BZ under constant volume conditions with zero static pressure. The results obtained from the harmonic and anharmonic phonon dispersion curves are labeled as 0 K (dotted line) and 600 K (solid line), respectively.

the present MD simulation is lower than the QHA prediction of 6.619 Å [41] or 6.608 Å [43]. Specifically, the present simulations capture the TO hardening at elevated temperature and agree well with experiments at 300 K [17], indicating that the thermal expansion considered here is reasonable and the overestimation of the volume by PBE is reduced. Figure 2(b) shows the calculated anharmonic phonon dispersion at 600 K. Compared to that at 300 K, it is apparent that phonon modes of the whole TO branch are sensitive to temperature. Their frequencies increase greatly with temperature such that the crossing between LA and TO modes disappears eventually, a phenomenon revealed by experimental and previous theoretical studies [17,20].

It is also interesting to explore the frequency shifts of phonon modes at finite temperature. Figure 2(c) displays the variation of frequency of the TO mode at the Γ point with temperature under constant volume conditions, which exhibits a discernible nonlinear behavior. It is known that the third-order many-body perturbation theory only predicts linear dependence of frequency shifts with temperature. Therefore, we conclude that the higher order anharmonic effects may play an important role here. For a direct comparison with experiments, we convert our data to the constant pressure conditions where $P = 0$ GPa by incorporating the temperature induced thermal expansion [24,33]. Figure 2(d) shows that our results are in good agreement with experiments.

With the obtained anharmonic phonon dispersions, the phonon group velocities can be evaluated as $v_{\mathbf{q},s} = d\omega_{\mathbf{q},s}/d\mathbf{q}$. Due to the giant frequency shifts, a significant variance of group velocities with temperature is expected. We have calculated group velocities at 600 K using anharmonic phonon dispersions and group velocities at 0 K using harmonic dispersions obtained with the DFPT approach. Figure 3 shows that although the phonon group velocities of acoustic modes do not vary much with temperature, the phonon group velocities of optical modes change to a great extent, especially for the TO branch. Here it is informative to note that such variation in group velocities with temperature is overlooked by the third order many-body perturbation theory in calculating κ_{lat} with the Boltzmann transport equation, Eq. (2).

C. Breakdown of the minimal mean free path theory in PbTe

According to the Peierls-Boltzmann theory [6–9], the heat transport property can be studied using the obtained phonon lifetime $\tau_{\mathbf{q},s}$. Figure 4(a) shows $\tau_{\mathbf{q},s}$ for all the phonon modes at those $\mathbf{q}$ sampled by the MD simulations at different temperatures. Overall, phonon lifetimes decrease with phonon frequencies. This can be understood from the relation [44]

$$1/\tau_{\mathbf{q},s} \propto \tilde{\omega}^2_{\mathbf{q},s}. \tag{7}$$

Equation (7) indicates that the lifetimes are short for phonons with high frequencies. Note that Eq. (7) was initially proposed for acoustic phonons. Later, it was applied to optical modes [45]. From Fig. 4(a), it can also be seen that phonon lifetimes are longer at 300 K than those at 600 K. This is common since anharmonic effects are stronger at higher temperature. For a better characterization of the behavior of phonon lifetimes, we study the temperature dependence of phonon lifetimes

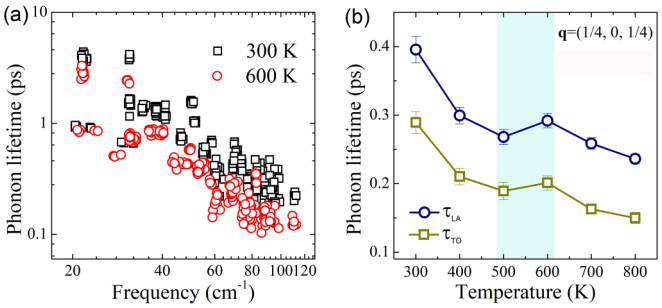

FIG. 4. (a) Phonon lifetimes (ps) of PbTe as a function of frequency at 300 K (black square) and 600 K (red circle), respectively, under constant volume conditions with zero static pressure. (b) The phonon lifetime of the TO and LA modes at $\mathbf{q} = (1/4,0,1/4)$ as a function of temperature under constant volume conditions with zero static pressure. The shaded area highlights the anomaly in the TO and LA modes.

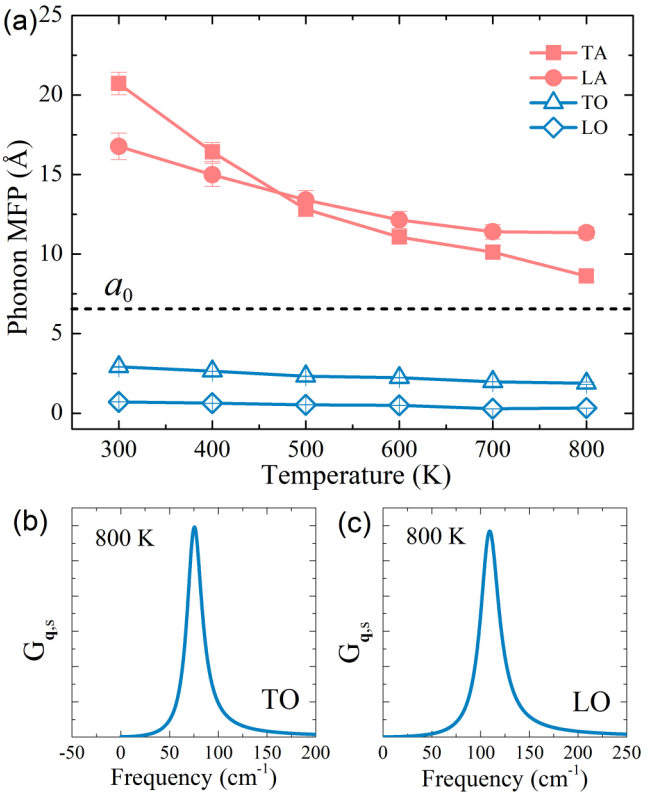

FIG. 5. (a) The dependence of the phonon MFP on temperature for different phonon modes at $\mathbf{q} = (\frac{1}{4},\frac{1}{4},\frac{1}{4})$ under constant volume conditions with zero static pressure. The horizontal dashed line indicates the lattice constant a_0. (b) and (c) show the power spectra for the TO and LO modes of $\mathbf{q} = (\frac{1}{4},\frac{1}{4},\frac{1}{4})$ at $T = 800$ K.

for individual modes. Figure 4(b) plots the lifetimes as a function of temperature of two modes: TO and LA at $\mathbf{q} = (\frac{1}{4},0,\frac{1}{4})$ where the TO branch and LA branch cross at low temperature, Fig. 2(a). Surprisingly, the descendant lifetimes curves versus the temperature of these two modes have a saddle at the temperature range roughly at $500 < T < 600$ K. This interesting phenomenon is interpreted as the consequence of the lifting of the degeneracy between the TO and the LA mode. At $T > 600$ K, the whole TO branch moves up with respect to the LA branch such that the crossing between the TO and LA branches disappears. As a result, the phonon-phonon scattering (anharmonic effect) of associated TO and LA modes are significantly reduced [17,20]. This result, once again, demonstrates the validity and accuracy of our approach.

We now use the obtained lifetimes to study the lattice thermal conduction of PbTe. Before proceeding, we first clarify a particular concept of the minimal thermal conductivity, which has been widely used as guidance in the search for materials with low thermal conductivity [46]. From Eq. (2), the lattice thermal conductivity κ_{lat} is closely related to the phonon mean free paths $l_{\mathbf{q},s}$. In general, $l_{\mathbf{q},s}$ might be very different for different phonon modes and decreases with temperatures. However, according to the so-called minimal mean free path theory [47,48], $l_{\mathbf{q},s}$ cannot be shorter than the lattice constants l_0, otherwise the phonon-phonon interactions are so strong that the phonon picture breaks, and when calculating κ_{lat} with Eq. (2), $l_{\mathbf{q},s}$ should be replaced with l_0 if $l_{\mathbf{q},s} < l_0$. Therefore, at sufficient high temperature, κ_{lat} approaches a minimal value.

Figure 5(a) shows that for the four modes: TA, LA, TO, and LO at $\mathbf{q} = (\frac{1}{4},\frac{1}{4},\frac{1}{4})$, while the phonon mean free paths of the two acoustic modes are longer than the lattice constants, the phonon mean free paths of the other two optical modes are much shorter than the lattice constants for the temperature considered here. According to the minimal mean free path theory, the phonon picture for these optical modes may be invalid. As a validity check, Figs. 5(b) and 5(c) show the power spectra for these two modes at $T = 800$ K. Both display the typical Lorantzian-type line shape with single peak, indicating that the concept of phonon quasiparticles is still valid even though their mean free paths are very short. This result demonstrates the breakdown of the minimal mean free path theory, i.e., there is no lower bound of phonon mean free paths, and, consequently, nor does the lattice thermal conductivity. We note that the difference in mean free paths between these optical modes and acoustic modes can be attributed to the fact that acoustic modes are of lower frequencies than optical modes such that their lifetimes are longer than those of optical modes.

We have calculated the lattice thermal conductivity κ_{lat} of PbTe covering the range of moderate temperature: $300 < T < 800$ K. The results are shown in Fig. 6. First of all, our calculated κ_{lat} roughly follows a $1/T$ scaling [Fig 6(a)], indicating that the abnormal behaviors of the TO and LA modes as shown in Fig. 4(b) have only negligible effect on thermal conduction. Here, it is interesting to note that, due to the nature of MD simulation, the obtained phonon lifetimes, $\tau_{\mathbf{q},s}$, and thus κ_{lat}, effectively capture the anharmonic effects to the infinite orders. On the contrary, some perturbation approaches usually consider only the third order of anharmonic coupling involving three-phonon scattering. Recently, Feng *et al.* [49] investigated the four-phonon scattering and showed that this higher order anharmonicity reduces lattice thermal conductivity to a great extent. As a result, κ_{lat} will decay with temperature faster than the well-known $1/T$ scaling. However, given our calculation, this result is odd and calls for further investigation in this aspect.

We have also collected the data given by previous experimental and theoretical reports [10,25,26,39,50–55] [Fig. 6(b)]. It is important to note that the thermal conductivity of PbTe

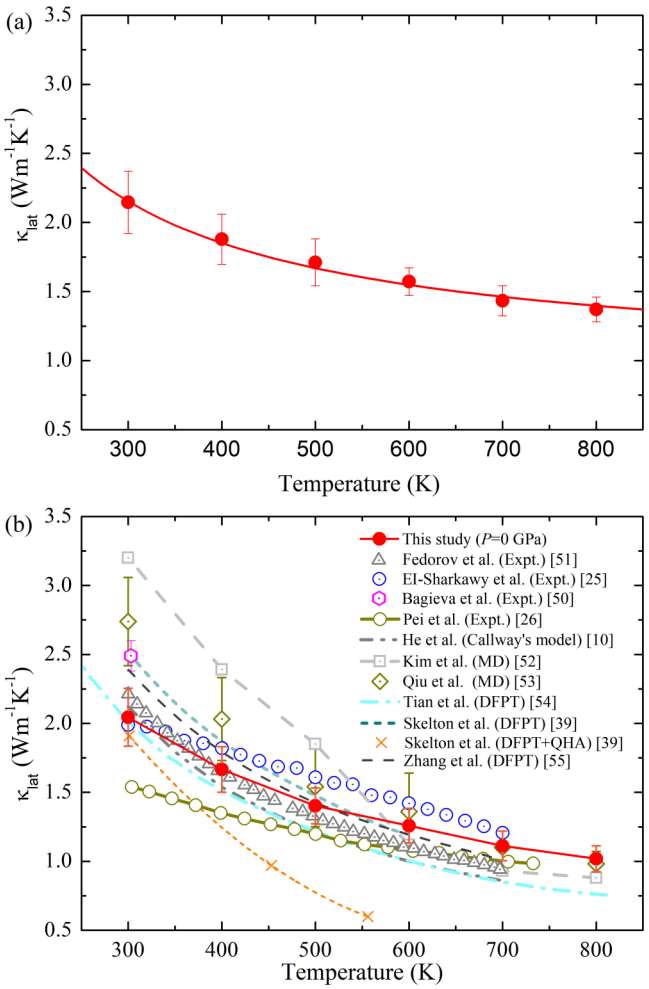

FIG. 6. Lattice thermal conductivity, κ_{lat}, of PbTe as a function of temperature (a) under constant volume conditions with zero static pressure, and (b) at pressure of $P = 0$ GPa (solid symbols). In (a), the solid line is a guide for the $1/T$ scaling. In (b), the experimental data of Fedorov and Machuev [51], EI-Sharkawy *et al.* [25], Bagieva *et al.* [50], and Pei and Liu [26], and the theoretical results of other investigators, i.e., He *et al.* [10], Kim and Kaviany [52], Qiu *et al.* [53], Tian *et al.* [54], Skelton *et al.* [39], and Zhang *et al.* [55] are shown for comparison.

has not been well constrained since these reported values are scattered in experiments. For example, at 300 K, EI-Sharkawy *et al.* reported the thermal conductivity of a polycrystalline PbTe sample with a value of $\kappa_{lat} \simeq 2.2$ W m^{-1} K^{-1} [25], Bagieva *et al.* reported a value of $\kappa_{lat} \simeq 2.38$–2.60 W m^{-1} K^{-1} for a single-crystal PbTe sample [50], and Pei and Liu reported a value of $\kappa_{lat} \simeq 1.54$ W m^{-1} K^{-1} [26]. We even further note that the reported theoretical κ_{lat} is even more dispersed [10,39,52–55]. Our calculated κ_{lat} fall in the coverage of experimental results.

IV. CONCLUSIONS

To summarize, the phonon gas model provides an excellent paradigm for the study of thermal property. In this work, we employ an approach which characterizes phonon quasiparticles from first-principles calculations to investigate the lattice dynamics of PbTe. Our calculation shows a strong anharmonic effect on both vibrational spectra and thermal conduction. The obtained anharmonic phonons dispersion with giant frequency shifts of TO modes are in good agreement with experiments [17] and other first-principles calculations [19,20]. In particular, we are able to capture the avoided crossing of TO and LA branches, and as a consequence, the abnormal behavior of phonon lifetimes of associated modes at the corresponding temperature. These aspects reveal the strong lattice anharmonicity in PbTe and demonstrate the accuracy of our approach. Further and more importantly, we showcase the breakdown of the minimal mean-free-path theory in the present system by showing that the phonon mean free paths can be shorter than lattice constants. The obtained lattice thermal conductivity is reasonable compared with experimentation.

ACKNOWLEDGMENTS

T.S. is supported by National Natural Science Foundation of China (NSFC) under Grant No. 41474069. D.B.Z. is supported by NSFC under Grant No. U1530401. Y.L. is supported by NSFC under Grants No. 11704020 and No. 11647010, the Higher Education and High-quality and World-class Universities (PY201611), and the BUCT Fund for Disciplines Construction (Project No. XK1702). Computation was performed at Beijing Computational Science Research Center.

APPENDIX

As a comparison of the phonon dispersion of PbTe, we carried out phonon calculations with both VASP and QE. At the Γ point, the frequency of the TO branch is 28.3 cm^{-1} given by VASP and 30.8 cm^{-1} given by QE, and the frequency of the LO branch is 108.9 cm^{-1} given by VASP and 111.3 cm^{-1} given by QE.

[1] H. J. Goldsmid, *Thermoelectric Refrigeration* (Plenum, New York, 1964).
[2] A. Majumdar, Science **303**, 777 (2004).
[3] L. D. Zhao, S. H. Lo, Y. S. Zhang, H. Sun, G. J. Tan, C. Uher, C. Wolverton, V. P. Dravid, and M. G. Kanatzidis, Nature (London) **508**, 373 (2014).
[4] Q. Zhang, E. K. Chere, Y. M. Wang, H. S. Kim, R. He, F. Cao, K. Dahal, D. Broido, G. Chen, and Z. F. Ren, Nano Energy **22**, 572 (2016).
[5] Z. W. Chen, Z. Z. Jian, W. Li, Y. J. Chang, B. H. Ge, R. Hanus, J. Yang, Y. Chen, M. X. Huang, G. J. Snyder, and Y. Z. Pei, Adv. Mater. **29**, 1606768 (2017).
[6] A. J. C. Ladd, B. Moran, and W. G. Hoover, Phys. Rev. B **34**, 5058 (1986).
[7] J. E. Turney, E. S. Landry, A. J. H. McGaughey, and C. H. Amon, Phys. Rev. B **79**, 064301 (2009).
[8] T. Sun and P. B. Allen, Phys. Rev. B **82**, 224305 (2010).

[9] X. L. Tang and J. J. Dong, Proc. Natl. Acad. Sci. USA **107**, 4539 (2009).

[10] J. Q. He, S. N. Girard, M. G. Kanatzidis, and V. P. Dravid, Adv. Funct. Mater. **20**, 764 (2010).

[11] Y. Pei, N. A. Heinz, A. LaLonde, and G. J. Snyder, Energy Environ. Sci. **4**, 3640 (2011).

[12] E. O. Wrasse, R. J. Baierle, T. M. Schmidt, and A. Fazzio, Phys. Rev. B **84**, 245324 (2011).

[13] Y. Z. Pei, H. Wang, and G. J. Snyder, Adv. Mater. **24**, 6125 (2012).

[14] S. A. Yamini, H. Wang, Z. M. Gibbs, Y. Z. Pei, S. X. Dou, and G. J. Snyder, Phys. Chem. Chem. Phys. **16**, 1835 (2014).

[15] G. A. Akhmedova and D. Sh. Abdinov, Inorg. Mater. **45**, 854 (2009).

[16] T. M. Tritt, *Thermal Conductivity: Theory, Properties, and Applications* (Kluwer Academic/Plenum Publishers, New York, 2004).

[17] O. Delaire, J. Ma, K. Marty, A. F. May, M. A. McGuire, M-H. Du, D. J. Singh, A. Podlesnyak, G. Ehlers, M. D. Lumsden, and B. C. Sales, Nat. Mater. **10**, 614 (2011).

[18] S. Lee, K. Esfarjani, T. Luo, J. Zhou, Z. Tian, and G. Chen, Nat. Commun. **5**, 3525 (2014).

[19] C. W. Li, O. Hellman, J. Ma, A. F. May, H. B. Cao, X. Chen, A. D. Christianson, G. Ehlers, D. J. Singh, B. C. Sales, and O. Delaire, Phys. Rev. Lett. **112**, 175501 (2014).

[20] A. H. Romero, E. K. U. Gross, M. J. Verstraete, and O. Hellman, Phys. Rev. B **91**, 214310 (2015).

[21] K. Esfarjani, G. Chen, and H. T. Stokes, Phys. Rev. B **84**, 085204 (2011).

[22] D.-B. Zhang, T. Sun, and R. M. Wentzcovitch, Phys. Rev. Lett. **112**, 058501 (2014).

[23] T. Sun, D.-B. Zhang, and R. M. Wentzcovitch, Phys. Rev. B **89**, 094109 (2014).

[24] E. S. Božin, C. D. Malliakas, P. Souvatzis, T. Proffen, N. A. Spaldin, M. G. Kanatzidis, and S. J. L. Billinge, Science **330**, 1660 (2010).

[25] A. A. EI-Sharkawy, A. M. Abou EI-Azm, M. I. Kenawy, A. S. Hillal, and H. M. Abu-Basha, Int. J. Thermophys. **4**, 261 (1983).

[26] Y. L. Pei and Y. Liu, J. Alloys Compd. **514**, 40 (2012).

[27] S. Baroni, P. Giannozzi, and A. Testa, Phys. Rev. Lett. **58**, 1861 (1987).

[28] S. Baroni, S. de Gironcoli, and A. Dal Corso, Rev. Mod. Phys. **73**, 515 (2001).

[29] P. E. Blöchl, Phys. Rev. B **50**, 17953 (1994).

[30] G. Kresse and J. Furthmüller, Phys. Rev. B **54**, 11169 (1996).

[31] J. P. Perdew, K. Burke, and M. Ernzerhof, Phys. Rev. Lett. **77**, 3865 (1996).

[32] H. J. Monkhorst and J. D. Pack, Phys. Rev. B **13**, 5188 (1976).

[33] S. Kastbjerg, N. Bindzus, M. Søndergaard, S. Johnsen, N. Lock, M. Christensen, M. Takata, M. A. Spackman, and B. B. Iversen, Adv. Funct. Mater. **23**, 5477 (2013).

[34] S. Nosé, Mol. Phys. **52**, 255 (1984).

[35] P. Giannozzi, S. Baroni, N. Bonini, M. Calandra, R. Car, C. Cavazzoni, D. Ceresoli, G. L. Chiarotti, M. Cococcioni, I. Dabo *et al.*, J. Phys.: Condens. Matter **21**, 395502 (2009); see http://www.quantum-espresso.org.

[36] Y. Zhang, X. Z. Ke, P. R. C. Kent, J. H. Yang, and C. F. Chen, Phys. Rev. Lett. **107**, 175503 (2011).

[37] T. Keiber, F. Bridges, and B. C. Sales, Phys. Rev. Lett. **111**, 095504 (2013).

[38] K. S. Knight, J. Phys.: Condens. Matter **26**, 385403 (2014).

[39] J. M. Skelton, S. C. Parker, A. Togo, I. Tanaka, and A. Walsh, Phys. Rev. B **89**, 205203 (2014).

[40] Y. Lu, T. Sun, Ping Zhang, P. Zhang, D.-B. Zhang, and R. M. Wentzcovitch, Phys. Rev. Lett. **118**, 145702 (2017).

[41] Y. Zhang, X. Z. Ke, C. F. Chen, J. Yang, and P. R. C. Kent, Phys. Rev. B **80**, 024304 (2009).

[42] J. E. Petersen, L. M. Scolfaro, and T. H. Myers, Mater. Chem. Phys. **146**, 472 (2014).

[43] J. M. Skelton, D. Tiana, S. C. Parker, A. Togo, I. Tanaka, and A. Walsh, J. Chem. Phys. **143**, 064710 (2015).

[44] P. Klemens, Proc. R. Soc. London, Ser. A **208**, 108 (1951).

[45] H. Dekura, T. Tsuchiya, and J. Tsuchiya, Phys. Rev. Lett. **110**, 025904 (2013).

[46] D. T. Morelli, *Thermoelectric Materials*, Springer Handbook of Electronic and Photonic Materials (Springer International Publishing, Cham, 2017).

[47] G. A. Slack, in *The Thermal Conductivity of Nonmetallic Crystals*, edited by H. Ehrenreich, F. Seitz, and D. Turnbull, Solid State Physics Vol. 34 (Academic Press, New York, 1979), pp. 1–71.

[48] C. Kittel, Phys. Rev. **75**, 972 (1949).

[49] T. Feng, L. Lindsay, and X. Ruan, Phys. Rev. B **96**, 161201 (2017).

[50] G. Z. Bagieva, G. M. Murtuzov, G. D. Abdinova, E. A. Allakhverdiev, and D. S. Abdinov, Inorg. Mater. **48**, 789 (2012).

[51] V. I. Fedorov and V. I. Machuev, Sov. Phys.-Solid State **11**, 1116 (1969).

[52] H. Kim and M. Kaviany, Phys. Rev. B **86**, 045213 (2012).

[53] B. Qiu, H. Bao, G. Q. Zhang, Y. Wu, and X. L. Ruan, Comp. Mater. Sci. **53**, 278 (2012).

[54] Z. Tian, J. Garg, K. Esfarjani, T. Shiga, J. Shiomi, and G. Chen, Phys. Rev. B **85**, 184303 (2012).

[55] Y. Zhang, J. J. Dong, P. R. C. Kent, J. H. Yang, and C. F. Chen, Phys. Rev. B **92**, 020301(R) (2015).